The Use of Geometric Diversity for Spectral Dominance in Underground Imaging

Lorenzo Lo Monte, Rashid Ansari, Danilo Erricolo
Department of Electrical and Computer Engineering
University of Illinois at Chicago
Chicago, IL 60607
lomonte@ece.uic.edu

Michael C. Wicks
Sensors Directorate
Air Force Research Laboratory
Rome, NY
Michael.wicks@rl.af.mil

***Abstract*—Underground imaging of dielectric and conductive anomalies performed using ground penetrating radars (GPRs) requires expensive wideband systems to increase the resolution. The advent of tomographic principles in multi-monostatic GPRs dramatically improved the imaging capabilities and suggested the possibility of reducing the bandwidth of the probing waveform. In this work we propose to extend the tomographic principles to the case of below-ground distributed sensing, thus taking advantage of the geometric diversity. We show that, by using geometric diversity, the frequency content required to image below-ground targets is drastically reduced to virtually a single monochromatic signal, thus achieving full spectral dominance in the waveform design.**

I. INTRODUCTION

Presently, a prevalent approach to detect, locate, trace and image underground objects is by using Ground Penetrating Radar [1]-[5]. Depth of penetration is augmented by logging data through boreholes. Image resolution is ameliorated by using tomographic principles applied to the received data [6]-[8]. However, all GPR systems need to use short pulses (i.e. high frequency bandwidth) to increase the information concerning the targets via frequency diversity.

The use of high bandwidth leads to several issues. First, the signal to noise ratio (SNR) decreases with an increase in the spectral content of the probing wavefield. Second, the electromagnetic spectrum available for military and civil applications is continuously being eroded due to the tremendous demand of wireless applications. Furthermore, unintentional (e.g. broadcasting stations) or intentional (e.g. jammers) man-made interferences can reduce the available spectrum. If larger bandwidth is required, EMI, EMC and intermodulation effects become difficult tasks to be tackled and solved. Third, a wideband system can be extremely bulky, delicate and expensive. This problem is accentuated when the system is designed to work at lower frequencies: it is impractical to generate well-designed short pulses in the HF frequency range, where antennas are fundamentally electrically small. Additionally, the shorter the pulse is, the greater is the difficulty and cost in properly sampling the received signal. Fourth, the conductivity and dielectric permittivity of the ground varies with the frequency: if a wideband signal is sent into the ground, frequency dispersion is likely to occur, thus broadening the pulse support and reducing the achievable resolution. Additional non-bandwidth related factors limit the efficiency of common GPRs. For example, the resolution in azimuth depends on the beamwidth: at HF frequencies it is impractical to create pencil beams, therefore azimuth resolution must be reduced by using other techniques. Moreover, common GPR suffer from the blind region effect in which the receiver is idle until the transmitter completes the transmission of the pulse. This problem can be solved by invoking suitable modulation techniques, at the penalty of increased complexity and cost of the system. Finally, when a target is not parallel to the surface, Euler's law suggests that reflected energy is not mainly back-propagating to the GPR receiver, and thus its detection may be compromised.

We propose a methodology [9]-[14], named RF tomography, that addresses these open issues, and we demonstrate how RF tomography may outperform current state-of-the-art GPR technology. RF tomography requires a set of low-cost penetrable transponders arbitrarily deployed above the ground (see Fig. 1). Transmitters send a waveform into the ground, scatterers re-irradiate power toward receivers, which log data and relay the retrieved information to a base station. The novelty of this approach is the use of multiple transmitters (i.e. view diversity) and multiple receivers (i.e. observation diversity), besides frequency, polarization and antenna pattern diversity. The accrual of geometric diversity facilitates the waveform frequency content reduction, and in the limiting case a set of discrete monochromatic signals yield actionable below-ground

 9781-4244-2971-4/09/$25.00©2009 IEEE

reconstructed images. In this work we focus on the inversion algorithms necessary to process the signals measured by the multitude of ground sensors.

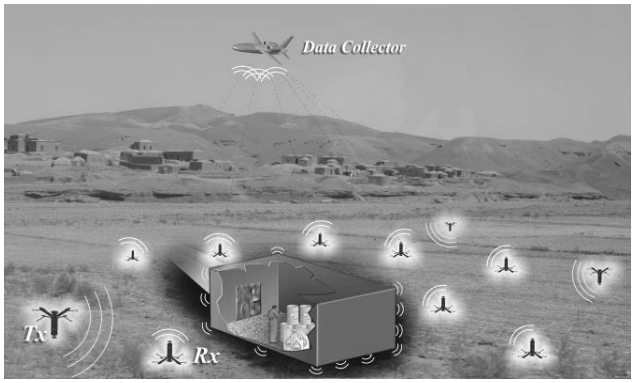

Figure 1: RF Tomography. Transmitters send power into the ground. Receivers collect the scattered field and send this information to the main station.

II. FORWARD MODEL

We describe the forward model of an RF tomographic system by considering the 3D geometry depicted in Fig. 2. The host medium (i.e. the earth) is modeled as an homogeneous medium with relative dielectric permittivity ε_D, conductivity σ_D, and magnetic permeability μ_0. The targets are assumed to reside in the investigation domain *D*. The sources are *N* electrically small dipoles (of length Δl^t) or loops (of area A^t) fed with current I^t, and located at position $\mathbf{r}_n^t$ (view diversity). For each transmitting antenna, the scattered field $\mathbf{E}^S$ is collected by *M* receivers (observation diversity), located at $\mathbf{r}_m^r$ points in space. For simplicity, a single operating frequency f is adopted.

We assume the relative dielectric permittivity profile $\varepsilon_r(\mathbf{r}')$ and the conductivity profile $\sigma(\mathbf{r}')$ inside the investigation domain *D* as unknowns of the problem.

Accordingly, the inverse problem is recast in terms of the unknown permittivity contrast function:

$$\varepsilon_\delta(\mathbf{r}') = \varepsilon_r(\mathbf{r}') - \varepsilon_D + j\frac{\sigma(\mathbf{r}') - \sigma_D}{2\pi f \varepsilon_0}. \quad (1)$$

In this way, the wave number inside *D* can be expressed as:

$$\begin{aligned} k^2(\mathbf{r}') &= \omega^2\mu_0\varepsilon_0\varepsilon_r(\mathbf{r}') + j\omega\mu_0\sigma(\mathbf{r}') \\ &= k_D^2 + k_0^2\varepsilon_\delta(\mathbf{r}') \end{aligned}, \quad (2)$$

$$\begin{aligned} k_D &= \omega\sqrt{\mu_0\varepsilon_0\varepsilon_D + j\mu_0\sigma_D/\omega} \\ k_0 &= \omega\sqrt{\mu_0\varepsilon_0} \end{aligned}. \quad (3)$$

The function in (1) accounts for the difference between the unknown dielectric permittivity of the object and that of the host medium.

For each point $\mathbf{r}'$ in region *D*, the vector wave equation holds:

$$\nabla\times\nabla\times\mathbf{E}(\mathbf{r}') = \left[k_D^2 + k_0^2\varepsilon_\delta(\mathbf{r}')\right]\mathbf{E}(\mathbf{r}'). \quad (4)$$

The scattered wave in a point $\mathbf{r} \notin D$ that is solution of (4) can be written in terms of integral equation of the dyadic Green's function:

$$\mathbf{E}^S(\mathbf{r}) = k_0^2 \iiint_D \underline{\underline{\mathbf{G}}}(\mathbf{r},\mathbf{r}')\cdot\mathbf{E}(\mathbf{r}')\varepsilon_\delta(\mathbf{r}')\,d\mathbf{r}', \quad (5)$$

where $\mathbf{E}(\mathbf{r}')$ is the total field in the investigation domain *D*, given as the superposition of the incident field $E^I(\mathbf{r}')$ (i.e. the field in the investigated area when objects are absent) and the field $\mathbf{E}^S(\mathbf{r})$, scattered by the targets.

As it is well known, the inverse scattering problem in (5) is non-linear. Nevertheless, it can be recast to a linear problem by means of the Born approximation (BA). Under BA, the total field inside the integrand of (5) can be approximated by the known incident field [15]-[18], i.e.:

$$\mathbf{E}^S(\mathbf{r}) \cong k_0^2 \iiint_D \underline{\underline{\mathbf{G}}}(\mathbf{r},\mathbf{r}')\cdot\mathbf{E}^I(\mathbf{r}')\varepsilon_\delta(\mathbf{r}')\,d\mathbf{r}'. \quad (6)$$

Therefore, the inverse problem at hand is cast as the inversion of the linear integral equation connecting the permittivity contrast function to the scattered field data.

The use of BA can be justified by considering that:

- The targets of interest are isolated, limited in number and embedded in a lossy medium. Therefore, mutual interaction (a phenomenon ignored by BA) between targets can be assumed negligible.
- In general, the inhomogeneities of the soil are electrically small, and their conductivity remains low. Therefore, their scattered fields are insignificant compared with the RF signal re-irradiated by our targets of interest.
- Our goal is to detect, localize and approximately determine the geometry of the targets. Toward this objective it has been shown how BA based inversion algorithms are able to work with strong scattering objects, provided that no quantitative description of the dielectric permittivity in *D* is required.

The Green's function depends upon the geometry that is considered (half-space, two-dimensional, full space). In this work, we utilize the three dimensional dyadic Green's function $\mathbf{G}$ for a homogeneous medium with the same properties of the earth. This assumption is reasonable because the sensors are deployed at the air/ground interface, and the frequencies involved are relatively low. Accordingly, we have [19]:

$$\underline{\underline{\mathbf{G}}}\left(\mathbf{r},\mathbf{r}'\right)=\left[\underline{\underline{\mathbf{I}}}+\frac{\nabla\nabla}{k_D^2}\right]\frac{e^{jk_D|\mathbf{r}-\mathbf{r}'|}}{4\pi|\mathbf{r}-\mathbf{r}'|}. \tag{7}$$

The operator $\nabla\nabla$ in (7), which is responsible for depolarization and is useful for near field sensing, can be generally neglected for $k_D|\mathbf{r}-\mathbf{r}'|>>1$, i.e. when sensors are located in the far zone with respect to targets.

The incident field, i.e. the field radiated in the homogeneous medium from a point source located at position $\mathbf{r}_n^t$, is given by:

$$\mathbf{E}_n^I\left(\mathbf{r}',\mathbf{r}_n^t\right)=Q\underline{\underline{\mathbf{G}}}\left(\mathbf{r}',\mathbf{r}_n^t\right)\cdot\hat{\mathbf{a}}_n^t, \tag{8}$$

where $Q=j\omega\mu_0\Delta l^t I^t$ for an electrically small dipole, or $Q=-j\omega\mu_0 A^t I^t$ for an electrically small loop, $\hat{\mathbf{a}}_n^t$ is the (electric or magnetic) dipole moment direction.

Additionally, the field received by a dipole or loop with moment direction $\hat{\mathbf{a}}_m^r$ positioned at $\mathbf{r}_m^r$ due to an equivalent (in terms of $\mathbf{E}_n^I$) current distribution defined inside the investigation domain *D* can be expressed as [28]:

$$E^S\left(\mathbf{r}_n^t,\mathbf{r}_m^r\right)=k_0^2\times \iiint_D \hat{\mathbf{a}}_m^r\cdot\underline{\underline{\mathbf{G}}}\left(\mathbf{r}_m^r,\mathbf{r}'\right)\cdot\mathbf{E}_n^I\left(\mathbf{r}',\mathbf{r}_n^t\right)\varepsilon_\delta\left(\mathbf{r}'\right)d\mathbf{r}'. \tag{9}$$

Substituting (8) in (9) we obtain the scalar forward model of RF tomography:

$$E^S\left(\mathbf{r}_n^t,\mathbf{r}_m^r\right)=\mathbf{L}\left(\varepsilon_\delta\left(\mathbf{r}'\right)\right)=Qk_0^2\times \iiint_D\left[\mathbf{a}_m^r\cdot\underline{\underline{\mathbf{G}}}\left(\mathbf{r}_m^r,\mathbf{r}'\right)\right]\cdot\left[\underline{\underline{\mathbf{G}}}\left(\mathbf{r}',\mathbf{r}_n^t\right)\cdot\mathbf{a}_n^t\right]\varepsilon_\delta\left(\mathbf{r}'\right)d\mathbf{r}'. \tag{10}$$

From a mathematical point of view, the problem of finding the contrast function is to perform the inverse of the linear operator $\mathbf{L}$ connecting the unknown contrast function and the scattered field data.

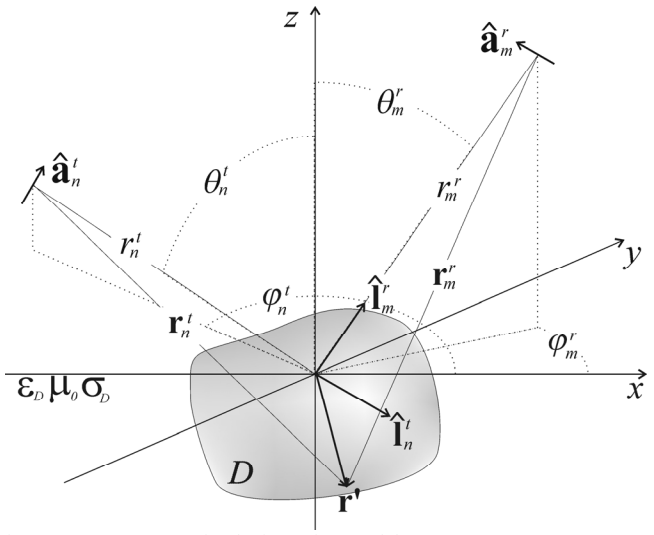

Figure 2: 3D Geometry for the inversion model.

III. INVERSION PROCEDURES

A. Tikhonov Regularization

A way to compute $\mathbf{L}^{-1}$ is to perform a numerical inversion of $\mathbf{L}$ [20]. Let us collect the sampled field data in an ordered *NM* vector $\underline{E}^S=\left\{E^S\left(\mathbf{r}_n^t,\mathbf{r}_m^r\right)\right\}$, and discretize the domain region *D* in *K* voxels, each one located at position $\mathbf{r}_k'$: the contrast dielectric permittivity can be embodied in a column vector $\underline{\varepsilon}_\delta=\left\{\varepsilon_\delta\left(\mathbf{r}_k'\right)\right\}$ of length *K*, and it represents the set of unknown parameters. After this discretization, eq. (10) can be rewritten in a matrix form:

$$\underline{E}^S=\underline{\underline{\mathbf{L}}}\underline{\varepsilon}_\delta, \tag{11}$$

where $\mathbf{L}$ now is a matrix with dimensions $NM\times K$.

The problem is then to invert the relation (11). Due to the independent set of measurements, $\mathbf{L}$ is theoretically full rank, but is often severely ill-conditioned. This leads to severe artifacts in the reconstruction process, particularly exacerbated when noise (thermal, external, quantization) or clutter is impinging the receivers.

A common way to quantify the behavior of $\mathbf{L}$ is by inspection of its condition number κ. For the operator $\mathbf{L}$ it is quite common to obtain typical values of κ above 10^6.

An efficient method to perform an inverse of a very ill conditioned matrix is by using the Tikhonov regularization procedure. In this way, the contrast dielectric permittivity can be estimated:

$$\hat{\underline{\varepsilon}}_\delta=\left(\mathbf{L}^H\mathbf{L}+\beta\mathbf{I}\right)^{-1}\mathbf{L}^H\underline{E}^S \tag{12}$$

Where $\mathbf{L}^H$ denotes the adjoint of $\mathbf{L}$, and β is the regularization parameter in the Tikhonov sense, that needs to be appropriately selected. The advantage of this approach is its remarkable performance in generating meaningful images, even when the number of sensors is limited. Unfortunately, a proper choice of β may be a difficult task, and often it is necessary to seek for a constrained optimization solution of β before a meaningful, sharp and low blurred image is reconstructed. This implies a (computationally expensive) matrix inversion for each attempt may be necessary.

B. Fourier Approach

In practical scenarios, where real-time processing is critical, or when the relay to a base-station is impeded, it is pivotal to derive an inversion strategy that privileges speed vs. accuracy. This priority is emphasized by the current system technology, which is widely implementing FFT routines to accelerate image reconstructions. Therefore, we propose an approach that takes advantage of the Fourier relation arising between scattered field and object shape, as discussed in literature under the topic of diffraction tomography.

In fact, if targets and sensors are distant enough so that the propagating wave is TEM (normally occurring when the fields are primarily propagating as $1/r$), then the forward model can be expressed as follows below.

We define the unit norm direction of propagation vectors as:

$$\hat{\mathbf{l}}_n^t = -\hat{\mathbf{x}}\sin\theta_n^t\cos\varphi_n^t - \hat{\mathbf{y}}\sin\theta_n^t\sin\varphi_n^t - \hat{\mathbf{z}}\cos\theta_n^t, \quad (13)$$

$$\hat{\mathbf{l}}_m^r = \hat{\mathbf{x}}\sin\theta_m^r\cos\varphi_m^r + \hat{\mathbf{y}}\sin\theta_m^r\sin\varphi_m^r + \hat{\mathbf{z}}\cos\theta_m^r. \quad (14)$$

Using the paraxial approximation, the transmitting Green's function at the generic position $\mathbf{r}'$ inside region *D* can be simplified as:

$$G_n^t\left(\mathbf{r}_n^t,\mathbf{r}'\right) \cong \frac{\exp\left(+jk_D r_n^t\right)\exp\left(+jk_D\hat{\mathbf{l}}_n^t\cdot\mathbf{r}'\right)}{4\pi r_n^t}, \quad (15)$$

while the receiving Green's function can be expressed as:

$$G_m^r\left(\mathbf{r}',\mathbf{r}_m^r\right) \cong \frac{\exp\left(+jk_D r_m^r\right)\exp\left(-jk_D\hat{\mathbf{l}}_m^r\cdot\mathbf{r}'\right)}{4\pi r_m^r}. \quad (16)$$

Therefore, for a pair of transmitters and receivers, the scatteres field can be rewritten as:

$$E^S\left(\mathbf{r}_n^t,\mathbf{r}_m^r\right) \cong \frac{k_0^2\hat{\mathbf{a}}_n^t\cdot\hat{\mathbf{a}}_m^r}{16\pi^2 r_n^t r_m^r}Qe^{+jk_D\left(r_r^t+r_m^r\right)}\times \iiint_D \varepsilon_\delta\left(\mathbf{r}'\right)\exp\left(+jk_D\left[\hat{\mathbf{l}}_n^t-\hat{\mathbf{l}}_m^r\right]\cdot\mathbf{r}'\right)d\mathbf{r}' \quad (17)$$

Eq. (17) is a simplified and continuous version of (10).

The quantity $k_D\left(\hat{\mathbf{l}}_n^t-\hat{\mathbf{l}}_m^r\right)$ can be represented by a 3D vector:

$$\mathbf{k}_{mn} = k_D\left(\hat{\mathbf{l}}_n^t-\hat{\mathbf{l}}_m^r\right). \quad (18)$$

Eq. (17) can be rewritten as [33]:

$$E^S\left(\mathbf{k}_{mn}\right) = \frac{k_0^2\hat{\mathbf{a}}_n^t\cdot\hat{\mathbf{a}}_m^r}{16\pi^2 r_n^t r_m^r}Qe^{+jk_D\left(r_m^t+r_n^r\right)}\times \iiint_D \varepsilon_\delta\left(\mathbf{r}'\right)\exp\left(+j\mathbf{k}_{mn}\cdot\mathbf{r}'\right)d\mathbf{r}' \quad (19)$$

It is useful to consider a normalized version of (19):

$$\bar{E}^S\left(\mathbf{k}_{mn}\right) = \frac{16\pi^2 r_n^t r_m^r}{Qk_0^2\hat{\mathbf{a}}_n^t\cdot\hat{\mathbf{a}}_m^r}e^{-jk_D\left(r_n^t+r_m^r\right)}E^S\left(\mathbf{k}_{mn}\right) = \iiint_D \varepsilon_\delta\left(\mathbf{r}'\right)\exp\left(+j\mathbf{k}_{mn}\cdot\mathbf{r}'\right)d\mathbf{r}' \quad (20)$$

This result can be interpreted in the following way: each collected sample $\bar{E}^S\left(\mathbf{k}_{mn}\right)$ returns the value of the $\mathbf{k}_{mn}$ spectral component of the contrast function $\varepsilon_\delta\left(\mathbf{r}'\right)$. Theoretically, if we have enough samples to fully populate the spectral representation of $\varepsilon_\delta\left(\mathbf{r}'\right)$, the discrete function $\bar{E}^S\left(\mathbf{k}_{mn}\right)$ in the limit can be approximated as a continuous function $\bar{E}^S\left(\mathbf{k}\right)$, and (20) can be interpreted as a 3D inverse Fourier transform of the permittivity contrast function. Therefore, we can reconstruct an image of the underground by direct Fourier transform eq. (19), i.e.:

$$\hat{\varepsilon}_\delta\left(\mathbf{r}'\right) = \iiint_K \bar{E}^S\left(\mathbf{k}\right)\exp\left(-j\mathbf{k}\cdot\mathbf{r}'\right)d\mathbf{k}, \quad (21)$$

where the domain of integration K is the support of $\bar{E}^S\left(\mathbf{k}\right)$. By inspection of (18), we conclude that when the sensors completely encircle the target, K is a sphere of radius $2k_D$, meaning that the available information of the

spectral content of $\varepsilon_\delta(\mathbf{r}')$ is limited up to the spectral component $2k_D$. Therefore, the reconstructed image of the contrast function will be a low-pass filtered version of the true image.

In the real scenario where a finite number of sensors are deployed, three factors affect the resolution (leading to blurring and artifacts): the invalidity of paraxial approximation, the non-uniform sampling, the sparse data set, and the attenuation constant.

In this work, we consider the attenuation to be negligible, so that the wave number in (21) remains a real quantity, and FFT can be applied.

Paraxial approximation holds when the angle $\theta_{\max}$ between the ray passing through the origin and the ray intersecting the boundary of the region *D* is negligible. This angle can be computed using:

$$\theta_{\max} = \max_j \left\{ \max_{\mathbf{r}' \in D} \left[\tan^{-1} \frac{\left| \mathbf{r}' - \left(\mathbf{r}' \cdot \hat{\mathbf{l}}_j \right) \hat{\mathbf{l}}_j \right|}{\left| r_j \hat{\mathbf{l}}_j + \left(\mathbf{r}' \cdot \hat{\mathbf{l}}_j \right) \hat{\mathbf{l}}_j \right|} \right] \right\}, \quad (22)$$

where *j* represents any transmitter or receiver. Blur reduction is accomplished by segmenting the region *D* into smaller analysis regions (where $\theta_{\max}$ remains small within the sub-region) and by considering an inverse problem (i.e. smaller FFT) for each sub-region. Then, the resulting sub-images are concatenated to form the final image.

The non-uniform to uniform grid transformation can be accomplished using *Tri-Linear* interpolation. Let us define a uniform grid in the spectral domain of the scattered field $\bar{E}(u,v,w)$, where:

$$u,v,w = -\frac{N_{x,y,z}}{2}\Delta k_{x,y,z}, -\left(\frac{N_{x,y,z}}{2}+1\right)\Delta k_{x,y,z}, \ldots, \frac{N_{x,y,z}}{2}\Delta k_{x,y,z} \quad (23)$$

For the tri-linear interpolation, let us define three intervals in the Fourier space: $\Delta\tilde{k}_x, \Delta\tilde{k}_y, \Delta\tilde{k}_z$. Let us consider a sample point (u,v,w) in the uniform grid to be estimated, and a non-uniform sample point $\mathbf{k}_{mn} = k_{mn}^x + k_{mn}^y + k_{mn}^z$ that has been measured: we can define an interpolation weighting factor as follows:

$$w_{mn}^{uvw} = h_x\left(k_{mn}^x - u\right) h_y\left(k_{mn}^y - v\right) h_z\left(k_{mn}^z - w\right) \quad (24)$$

where:

$$h_{x,y,z}(a) = \begin{cases} 1 - \dfrac{|a|}{\Delta\tilde{k}_{x,y,z}} & |a| \le \Delta\tilde{k}_{x,y,z} \\ 0 \quad \text{otherwise} \end{cases} \quad (25)$$

The total weighting factor is:

$$W^{uvw} = \sum_{n=1}^{N}\sum_{m=1}^{M} w_{mn}^{uvw} \quad (26)$$

The estimated value in (u,v,w) is therefore:

$$\bar{E}(u,v,w) = \frac{1}{W^{uvw}} \sum_{n=1}^{N}\sum_{m=1}^{M} w_{mn}^{uvw} \bar{E}\left(\mathbf{k}_{mn}\right) \quad (27)$$

The major advantage of this technique is the intrinsic possibility of estimate missing samples when we choose $\Delta\tilde{k}_{x,y,z} > \Delta k_{x,y,z}$. In this way, the reconstructed image shows fewer artifacts and fewer oscillations.

A way to recover information from the missing samples on the sparse dataset can be accomplished by using the technique of Projection on Convex set (POCS). The basic idea of POCS is to properly weight the available samples in a way that the correspondent point spread function is minimized. The *ideal* point spread function (PSF)

$$PSF(\mathbf{r}') = \sum_{u^2+v^2+w^2 \le 2k_D} e^{-(jux'+vy'+wz')} \Delta k_x \Delta k_y \Delta k_z \quad (28)$$

coincides with the impulse response of the RF tomography optical system, i.e. has the shape of a 3D Bessel-sinc function, and it can be computed numerically by using a 3D FFT algorithm so that the PSF is known for any value of $\mathbf{r}'$ in the region D. For simplicity, let us consider an equivalent scaled problem in which $u,v,w \in \mathbb{Z}$ and $\Delta k_x \Delta k_y \Delta k_z = 1$

However, the *actual* PSF generated by the $S \le N_x N_y N_z$ available samples is:

$$\overline{PSF}(\mathbf{r}') = \sum_{s=1}^{S} p_s e^{-j(u_s x' + v_s y' + w_s z')} \quad (29)$$

where the weighting factors p_s are identically equal to unity. In principle, by properly weighting the elements in the incomplete summation (29), it may be possible that the weighted actual PSF is *pointwise* very similar to the ideal PSF:

$$\overline{PSF}\left(x',y',z'\right) \cong PSF\left(x',y',z'\right) \qquad (30)$$

In order to achieve this result we invoke the Projection on Convex Sets method, which is based on successive approximations of the actual PSF until a stopping criterion is met.

In the first iteration, we estimate the point spread function by imposing all weights to be $p_S = 1$. The next step is to compare *pointwise* the computed PSF with the ideal PSF (in the Space domain). More exactly, we create a suitable *guard band region* on the ideal PSF. If the values of the actual PSF are falling outside the guard region, we force these values to be inside the guard region. Once the corrections on the computed PSF are done, we perform a 3D IFFT. The Fourier transform of the *corrected* actual PSF is generally a function that has values for any u, v, w pairs. The next step is to set to zero all points in the Fourier domain that represent our missing samples. In this way, we are creating a new function defined only where actual samples are located.

We perform a new computation of PSF using the values p_s previously obtained, and the POCS iteration continues from until a stopping criterion is met, e.g. the computed PSF lies completely within the guard band region, or the *n*-th iteration of the computed PSF does not improve the approximation of the ideal PSF with respect of the n-1th iteration, i.e. the process stalls.

When POCS terminates, the coefficient p_s of the last iteration are used for computing the non-uniform inverse Fourier transform of the received electric field, as follows:

$$\hat{\varepsilon}_\delta\left(\mathbf{r}'\right) = \sum_{s=1}^{S} p_s e^{-j\left(u_s x' + v_s y' + w_s z'\right)} \overline{E}\left(u_s, v_s, w_s\right) \qquad (31)$$

IV. Simulations and Results

We performed several simulations using the methods described above. The geometry is depicted in Fig. 3, the probing frequency is 3MHz, and results are shown in Figs. 4,5,6. Considerations and further examples will be shown at the time of the conference.

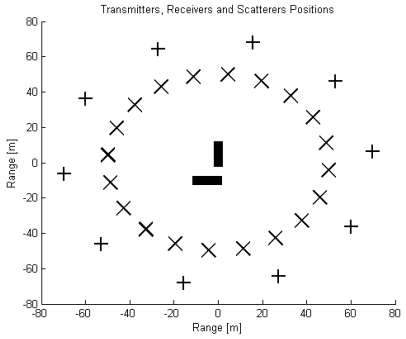

Figure 3: : Geometry for the simulation (top view). Transmitters are represented with "+", while receivers are represented with "X". The two black lines represent the positions of the tunnels.

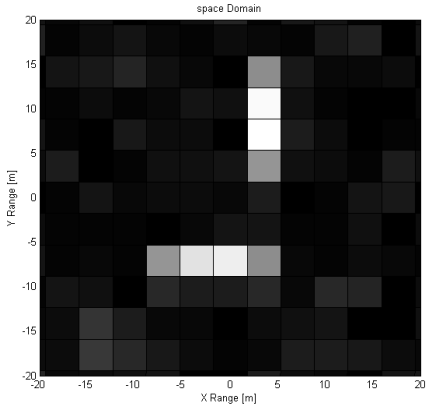

Figure 4: reconstructed image using Fourier, no POCS

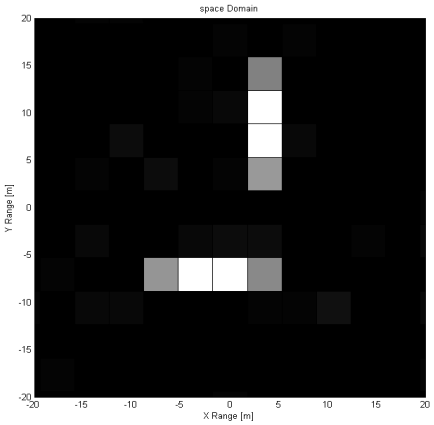

Figure 5: reconstructed image using Fourier and POCS

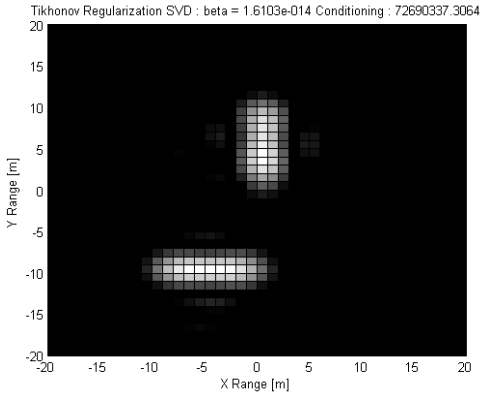

Figure 6: reconstructed image using Tikhonov

V. Acknoweledgements

The authors are thankful to Mr. W. Baldygo, Air Force Research Laboratory, for sponsoring and funding this research. We are also grateful to Mr. J. Parker, Dr. M. Ferrara, Air Force Research Laboratory, Dr. F. Soldovieri, Consiglio Nazionale Ricerche, Italy, Prof. M. Cheney, Rensselaer Polytechnic Institute, for their technical discussions.

REFERENCES

[1] R.J. Lytle, E.F Laine, D.L. Lager and D.J. Davis "Using Cross Borehole Electromagnetic Probing to Locate High Contrast Anomalies," Geophysics. Vol. 44, pp. 1667-1676, 1979.

[2] A.J Devaney, "Geophysical Diffraction Tomography" IEEE Trans on Geosci. Remote Sens. Vol. GE-22, No. 1, pp. 3-13, Jan. 1984.

[3] D. J. Daniels, *Ground Penetrating Radars, Second Edition.* Institution of Electrical Engineers, London, UK, 2004.

[4] A.J. Witten, J.E. Molyneux, J.E. Nyquist, "Ground Penetrating Radar Tomography: Algorithms and Case Studies," *IEEE Trans. Geosci. Remote Sens.,* Vol 32, No. 2, pp. 461-467, Mar. 1994.

[5] A.J. Witten, and E. Long, "Shallow Applications of Geophysical Diffraction Tomography". *IEEE Transactions on Geoscience and Remote Sens.,* Vol. 24, No. 5, p. 654-662, Sept. 1986

[6] T. B. Hansen, and P. M. Johansen, "Inversion Scheme for Ground Penetrating Radar that Takes Into Account the Planar Air-Soil Interface," *IEEE Trans. Geosci. Remote Sens.,* Vol. 38, No. 1, pp. 496-506, Jan. 2000

[7] T. J. Cui and W. C. Chew, "Diffraction Tomographic Algorithm for the Detection of Three-Dimensional Objects Buried in a Lossy Half-Space," *IEEE Transactions on Antennas and Propagation.* Vol. 50, No. 1, pp. 42-49, Jan. 2002.

[8] P. Meincke, "Linear GPR Inversion for Lossy Soil and a Planar Air-Soil Interface," *IEEE Trans. Geosci. and Remote Sens.*, Vol 39, No. 12, pp. 2713-2721, Dec. 2001

[9] M. C. Wicks, "RF Tomography with Application to Ground Penetrating Radars," *IEEE Proc. 41st Asilomar Conference ACSSC 2007*, pp. 2017-2022, 4-7 Nov. 2007

[10] L. Lo Monte, D. Erricolo, and M. C. Wicks, "Propagation Model, Optimal Geometry and Receiver Design for RF Geotomography," *IEEE Proc. RadarCon 2008,* Rome, Italy, May 26-30, 2008.

[11] L. Lo Monte, A. M. Bagci, D. Erricolo, and R. Ansari, "Spatial Resolution in Tomographic Imaging with Diffracted Fields," *Proc. XXIX General Assembly of the International Union of Radio Science (URSI),* Chicago, IL, USA, Aug. 7-16, 2008.

[12] L. Lo Monte, and D. Erricolo, "Distributed RF Tomography for Voids Detection," *Proc. 2008 Meeting for the Military Sensing Symposia (MSS), Specialty on Battlespace Acoustic and Seismic Sensing, Magnetic and Electric Field Sensors,* Laurel, MD, USA, Aug. 19-21, 2008.

[13] J. Norgard, M.C. Wicks, and A. Drozd, "Distributed/Embedded Sub-Surface Sensors for Imaging Buried Objects with Reduced Mutual Coupling and Suppressed Electromagnetic Emissions," *Proc. International Conference on Electromagnetics in Advanced Applications (ICEAA),* pp. 427-430, Turin, Sept. 17-21 2007.

[14] L. Lo Monte, and D. Erricolo, "Receiving Antenna Design for Ground Penetrating Tomographic Imaging", *Proc. IEEE AP-S International Symposium*, San Diego, CA, USA, Jul. 5-12, pp. 1-4, 2008.

[15] G. Leone, F. Soldovieri, "*Analysis of the distorted Born approximation for Subsurface Reconstruction: Truncation and Uncertainities Effect,"* IEEE Trans. on Geosci. and Remote Sens., Vol. 41, No. 1, pp. 66-74, Jan. 2003

[16] R. Persico, R. Bernini, F. Soldovieri, "The Role of the Measurement Configuration in Inverse Scattering from Buried Objects under the Born Approximation," *IEEE Trans on Antennas Propag.,* Vol. 53, No. 6, pp. 1875-1887, Jun 2005

[17] H. J. Li and F. L. Lin, "A Generalized Interpretation and Prediction in Microwave Imaging Involving Frequency and Angular Diversity," *J. Electromagnetic Waves and Applications*, Vol. 4, No. 5, pp. 415-430, 1990

[18] F. Soldovieri, J. Hugenschmidt, R. Persico, G. Leone, "A Linear Inverse Scattering Algorithm for Realistic GPR Applications," *Near Surface Geophysics*, Vol. 5, No. 1, pp. 29-42, Feb. 2007

[19] W.C. Chew, *Waves and Fields in Inhomogeneous Media*. IEEE Press, 1995, Piscataway NJ

[20] M. Bertero, and P. Boccacci, *Introduction to Inverse Problems in Imaging,* Institute of Physics Ltd, London, UK, 2002.